




HCO⁺ Dissociative Recombination: A Significant Driver of Nonthermal Hydrogen Loss at Mars

Bethan S. Gregory¹ , Rodney D. Elliott¹, Justin Deighan¹ , Hannes Gröller², and Michael S. Chaffin¹ 

¹Laboratory for Atmospheric and Space Physics, University of Colorado Boulder, Boulder, CO, USA, ²Lunar and Planetary Laboratory, University of Arizona, Tucson, AZ, USA

Key Points:

- We investigate nonthermal hydrogen escape via HCO⁺ dissociative recombination for the first time
- This is likely the dominant nonthermal mechanism, potentially responsible for >50% of the total escape under certain conditions
- Though important for H loss, we predict that this mechanism impacts brightness negligibly, posing a challenge for spacecraft observations

Supporting Information:

Supporting Information may be found in the online version of this article.

Correspondence to:

B. S. Gregory,
bethan.gregory@colorado.edu

Citation:

Gregory, B. S., Elliott, R. D., Deighan, J., Gröller, H., & Chaffin, M. S. (2023). HCO⁺ dissociative recombination: A significant driver of nonthermal hydrogen loss at Mars. *Journal of Geophysical Research: Planets*, 128, e2022JE007576. <https://doi.org/10.1029/2022JE007576>

Received 12 SEP 2022

Accepted 5 JAN 2023

Abstract Hydrogen escape to space has shaped Mars' atmospheric evolution, driving significant water loss. An unknown fraction of atmospheric H lost acquires its escape energy from photochemical processes, with multiple observational studies suggesting much higher densities of such “hot” H than models predict. Here, we show that a previously unconsidered mechanism, HCO⁺ dissociative recombination, produces more escaping hot H than any previously studied process, potentially accounting for more than 50% of escape during solar minimum aphelion conditions and ~5% of the expected long-term average loss. This hot H is predicted to impact observed brightness profiles negligibly, posing a significant challenge to the interpretation of spacecraft remote sensing observations. This mechanism's efficiency is largely due to the high (63%–83%) albedo of the planet to H at 1–10 eV energies, indicating the likely importance of dozens of similar photochemical mechanisms for the desiccation of Mars, Venus and planets throughout the universe.

Plain Language Summary The escape of hydrogen atoms from the upper atmosphere of Mars has led to significant loss of water from the planet. Hydrogen needs energy to escape Mars' gravitational pull, which can be sourced from the energy given to H atoms when they are produced by chemical reactions—this results in “hot” hydrogen. However, the importance of hot hydrogen escape is unknown, and there is a disparity between predictions from observations and models. Here, we show that one reaction, HCO⁺ dissociative recombination (HCO⁺ + e⁻ → CO + H), which has never been considered before, produces more escaping hot H than any process previously studied. In some seasonal conditions, it accounts for more than half the H loss, while accounting for 5% on longer timescales. Despite its importance, we predict that the hot H produced by this process is very difficult for spacecraft to observe. This mechanism is effective for escape because most H atoms produced by chemical reactions at high altitudes escape, so dozens of similar mechanisms are likely to be important at Mars. HCO⁺ dissociative recombination is probably significant at Venus, where hot H escape is dominant, and perhaps at other rocky planets outside the solar system.

1. Hot H Loss at Mars: A Significant Knowledge Gap

Escape of atomic hydrogen to space, a process responsible for the depletion of a large proportion of Mars' primordial water inventory, has sculpted the planet's atmospheric evolution (Anderson & Hord, 1971; Owen et al., 1988; Villanueva et al., 2015). The dominant mechanism for hydrogen loss at Mars is thought to be thermal (Jeans) escape, in which a small proportion of hydrogen atoms with velocities in the high-energy tail of a collisional velocity distribution have sufficient energy to escape the planet's gravity. Existing thermal H escape estimates include fluxes of $1.4 \times 10^8 \text{ cm}^{-2} \text{ s}^{-1}$ and $1.8 \times 10^8 \text{ cm}^{-2} \text{ s}^{-1}$, retrieved from Lyman alpha observations, assuming one population of thermal hydrogen (Anderson & Hord, 1971; Chaufray et al., 2008), and a flux of $2.4 \times 10^8 \text{ cm}^{-2} \text{ s}^{-1}$, given by the photochemical model of Nair et al. (1994), balancing the atomic oxygen sinks (Lammer et al., 2003). On seasonal timescales, thermal hydrogen escape varies between $0.1\text{--}50 \times 10^8 \text{ cm}^{-2} \text{ s}^{-1}$ (Bhattacharyya, Clarke, Chaufray, et al., 2017; Bhattacharyya et al., 2015; Chaffin et al., 2014; Chaufray et al., 2021; Clarke et al., 2014; Halekas, 2017). Seasonal H escape is dependent on mesospheric and thermospheric water vapor concentrations (Heavens et al., 2018; Krasnopolsky, 2019; Stone et al., 2020), which are driven by temperature variations and enhanced by dust events, as observed by instruments on several spacecraft (Aoki et al., 2019; Chaffin et al., 2021; Federova et al., 2018, 2020) and shown by photochemical (Chaffin et al., 2017) and global circulation modeling (Neary et al., 2020; Shaposhnikov et al., 2019).

Despite the significance of thermal H escape, the presence of a second, smaller population of higher-temperature hydrogen atoms—nonthermal or “hot” hydrogen—has been indicated by modeling studies (e.g., Nagy et al., 1990) and inferred by spacecraft observations (Bhattacharyya et al., 2015; Chaffin et al., 2018; Chaufray et al., 2008; Galli et al., 2006; Lichtenegger et al., 2006). These particles gain an energy boost through either the exothermic photochemical reactions by which they are formed or momentum or charge exchange processes. The relative importance of thermal and nonthermal H escape has yet to be definitively established (Bhattacharyya et al., 2015). Nagy et al. (1990) were the first to model hot H densities around Mars, through production by charge exchanges of energetic H ions with neutral O or H atoms. They computed a hot hydrogen abundance more than two orders of magnitude lower than its thermal counterpart, suggesting negligible nonthermal escape. Inclusion of five additional H-producing reactions resulted in slightly higher predicted exospheric densities (Lichtenegger et al., 2006). Krasnopolsky (2010) calculated H loss after photochemical production to be 3%–4% of the thermal H loss, assuming all hot H produced above the exobase escapes, and momentum transfer with nonthermal O accounted for escape equal to 5% of thermal escape in the model of Shematovich (2013). However, recent observations of the H corona by the Hubble Space Telescope and Mars Express suggest the presence of a larger nonthermal component, perhaps 8%–50% of the thermal H density (Bhattacharyya et al., 2015; Chaufray et al., 2008; Galli et al., 2006). The abundance ratio is not the same as the ratio of escape fluxes; some predictions result in a nonthermal escape contribution of almost half the total (Bhattacharyya, Clarke, Bertaux, et al., 2017; Bhattacharyya, Clarke, Chaufray, et al., 2017; Bhattacharyya et al., 2015), while Chaffin et al.'s (2018) two-population model reproduced Mars Atmosphere Volatile and Evolution (MAVEN) Lyman alpha measurements with a hot to thermal H density ratio of only 1%, consistent with Nagy et al. (1990), but resulting in hot H escape of 5%–25% that of total escape. The discrepancy between model predictions and empirical observations motivates a reassessment of H loss, especially as some nonthermal H-producing mechanisms have not been included in existing models.

In this study, we use a new Monte Carlo model, based on those of Lillis et al. (2017) and Gröller et al. (2010, 2012, 2014), but completely reimplemented here, to quantify nonthermal H escape at Mars via HCO⁺ dissociative recombination. We choose this mechanism because HCO⁺ is the dominant H-bearing ion in the upper atmosphere (Fox, 2015; Krasnopolsky, 2002; Matta et al., 2013), yet its influence on escape has not been explored. Secondly, we report hot H escape probability profiles at Mars, which can be used to quantify loss via any similarly energetic photochemical mechanism whose H production rates are known.

2. Monte Carlo Model

Our new Monte Carlo model (Figure 1) tracks a number of test particles, representative of a hot H population, as they move through the atmosphere, allowing the calculation of escape rates, coronal density structure, and energy distributions. Related models have previously been used to quantify nonthermal O and C escape at Mars (Gröller et al., 2014; Lillis et al., 2017). More generally, Monte Carlo techniques have been implemented for decades to simulate particle trajectories in the upper atmospheres of planetary bodies (e.g., Amerstorfer et al., 2017; Bougher et al., 2008; Chaufray et al., 2007; Hodges, 1994, 1999; Hodges & Tinsley, 1986; Johnson et al., 2008; Lichtenegger et al., 2006).

The test particles are initially distributed with altitude according to an input production rate profile, with initial velocities dependent on the excess energy of the simulated mechanism and isotropically distributed in direction. The model tracks the particles' positions as they respond to gravity and collide elastically with neutral background species (CO, CO₂, N₂, and O). We use the total and differential O–H cross sections of Zhang et al. (2009), without modification, for collisions with all four background species due to a lack of availability of more specific data. The cross sections are energy-dependent, and the collision energy is the sum of the kinetic energies of the H and the ambient background species in the center of mass reference frame, where the velocity of the background particle is randomly sampled from a Maxwell-Boltzmann distribution at the neutral temperature at the collision altitude (with temperature profiles from Fox (2015)). A collision is simulated if a random number from a uniform distribution between 0 and 1 is greater than $\sum e^{-\sigma_s n_s v \Delta t}$, where, for each background species, σ_s is the total cross section at the collision energy, n_s is the density at the collision altitude, v is the test particle velocity, and Δt is the timestep. The background particle involved in the collision is chosen randomly with relative probability based on the contribution of each species to this collision depth. To compute the outgoing angle, the differential cross section for the energy closest to the computed energy (from 0.1, 0.5, 1, or 5 eV) is used. A probability distribution function, derived from the differential cross section, is randomly sampled to select the scattering angle. When

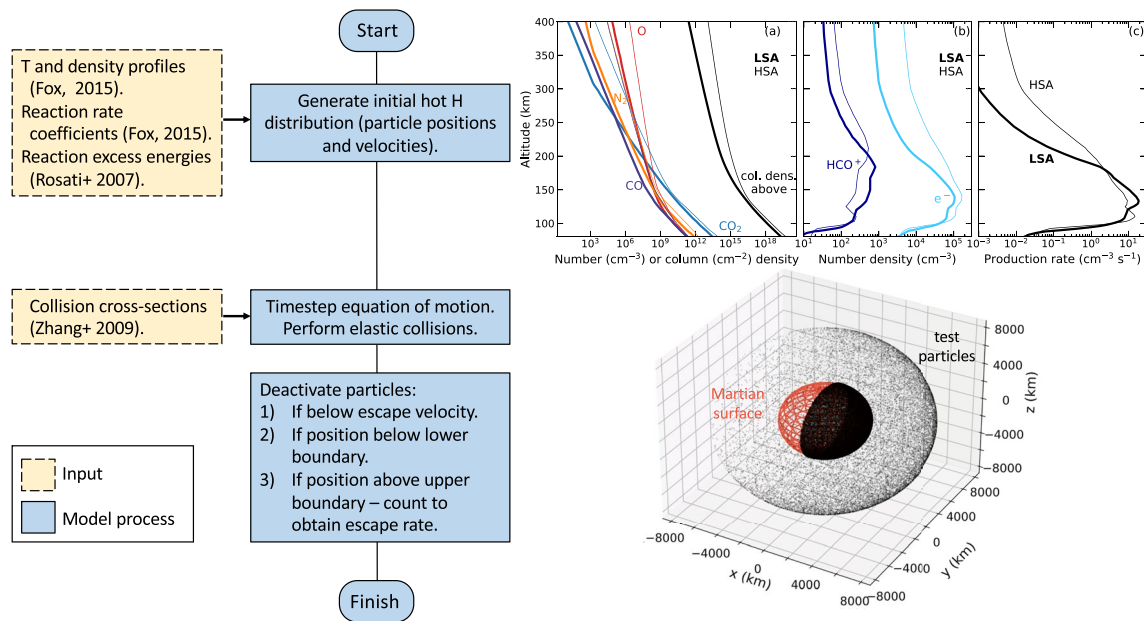


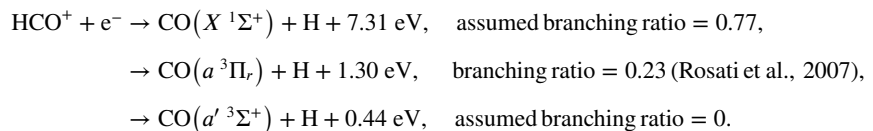
Figure 1. Schematic summarizing model inputs, processes, and outputs. Left-hand panel: flowchart of Monte Carlo model inputs (yellow boxes) and processes (blue boxes). Top right: (a) input density profiles of background species. Black lines show total column density above each altitude. (b) Input density profiles of HCO^+ (dark blue) and electrons (bright blue). Densities in (a, b) are from Fox (2015), for low (thick lines) and high (thin lines) solar activity. (c) Hot H production rate profiles due to HCO^+ dissociative recombination, which direct the initial hot H distribution, for low (thick line) and high (thin line) solar activity. Lower right: positions of test particles (black points) in the model at the end of a simulation; positive x coordinates are on the dayside. Hot H densities are higher in the dayside hemisphere because HCO^+ dissociative recombination is an ionospheric process that occurs only on the dayside.

a collision occurs, the particle's velocity vector is updated accordingly. We neglect inelastic collisions as they are unimportant relative to elastic collisions at the low energies relevant to H scattering through an atmosphere predominantly composed of much heavier species (Lichtenegger et al., 2006).

The simulation ends when all test particles are “deactivated” through one of three conditions: (a) the particle is thermalized (i.e., its energy falls below the escape energy (between 0.05 eV at the upper boundary (5,000 km) and 0.13 eV at the lower boundary (80 km)), (b) the particle's position moves below the lower boundary, or (c) the particle reaches the upper boundary with an energy greater than or equal to the escape energy. Those in category (c) are counted, and the fraction is multiplied by a dayside hemispheric production rate to give a global escape rate. As well as escape fractions, hot H density and energy distributions are calculated following tallying methods utilized by previous Monte Carlo models (X-5 Monte Carlo Team, 2003; see Supporting Information S1).

3. Significant Nonthermal H Escape From HCO^+ Dissociative Recombination

We use the model to calculate escape rates of H produced via the dissociative recombination of HCO^+ . Assuming that all HCO^+ and H is in the ground state, the branches of this reaction are:



(Rosati et al., 2007). Most of the excess energy—1.30 or 7.31 eV, depending on the electronic state of the CO (Rosati et al., 2007)—goes into the H atom's velocity, resulting in “hot” hydrogen with energies far above the escape energy at production altitudes (0.12–0.13 eV). This velocity is compounded with the velocity of the center of mass of the reactants:

$$\frac{m_1 u_1 + m_2 u_2}{m_1 + m_2} \quad (1)$$

to obtain the initial velocity of the H atom, where m_1 and m_2 are the masses of HCO^+ and an electron, respectively, and v_1 and v_2 are their velocities. For each initialized H particle, the reactant velocities are chosen by randomly sampling a Maxwell-Boltzmann distribution at the ion or electron temperature (from Fox, 2015) at the collision altitude.

The model initializes 100,000 test H particles, with positions dictated by the HCO^+ dissociative recombination production rate profile between 80 and 400 km (Figure 1), which is assumed to be uniform across the dayside. Production is calculated for both low (LSA) and high (HSA) solar activity conditions using HCO^+ and electron density profiles from Fox's (2015) eroded model. The low and high solar activity conditions are defined by Fox (2015) and characterized by a solar zenith angle of 60° , an orbital distance of 1.524 AU, and $F_{10.7}$ values of 68 and 214, respectively. The input HCO^+ profiles show peak densities of $8.1 \times 10^2 \text{ cm}^{-3}$ and $5.3 \times 10^2 \text{ cm}^{-3}$ at altitudes of 185 and 208 km, for low and high solar activity conditions, respectively (Fox, 2015), resulting in lifetimes of 523 and 998 s at the peaks, respectively. The dominant sink of HCO^+ in Mars' upper atmosphere is dissociative recombination, while two reactions involving OCOH^+ are among the most important source mechanisms (Fox, 2015; Krasnopolsky, 2002, 2019). We use the rate coefficients adopted by Fox (2015): $2 \times 10^{-7} (T_e/300)^{-1.25} \text{ cm}^3 \text{ s}^{-1}$ for $T_e \leq 300 \text{ K}$ and $2 \times 10^{-7} (T_e/300)^{-1.00} \text{ cm}^3 \text{ s}^{-1}$ for $T_e > 300 \text{ K}$, where T_e is the electron temperature (Fox, 2015). We adopt the $\text{CO}(a)$ yield of 23% reported by Rosati et al. (2007) and assume that ground state $\text{CO}(X)$ is produced 77% of the time, with a branching ratio of zero to the excited $\text{CO}(a')$ state. We account for the probabilities of $\text{CO}(a)$ with different vibrational levels after Rosati et al. (2007; 0.45 for $v = 0$, 0.21 for $v = 1$, 0.13 for $v = 2$, 0.10 for $v = 3$, and 0.10 for $v = 4$), but neglect different vibrational levels for the $\text{CO}(X)$ branch, as none were reported. After accounting for the CO molecule's electronic and vibrational states, the CO and H gain all remaining exothermic energy from recombination as translational kinetic energy, using conservation of momentum in the center of mass frame.

We predict escape rates for HCO^+ dissociative recombination by running a series of 10 simulations. The mean output global escape rates (Figure 2) are $1.30 \pm 0.01 \times 10^{25} \text{ s}^{-1}$ and $6.92 \pm 0.04 \times 10^{24} \text{ s}^{-1}$ for low and high solar activity, respectively. These values correspond to 6.5% and 3.5% of Nair et al.'s (1994) thermal escape flux, $2.4 \times 10^8 \text{ cm}^{-2} \text{ s}^{-1}$ (equal to a global loss rate of $2 \times 10^{26} \text{ s}^{-1}$). This is comparable to previous forward model-based photochemical loss fractions (3%–5%; Krasnopolsky, 2010; Shematovich, 2013), which did not include HCO^+ dissociative recombination. Inclusion of this new mechanism would therefore roughly double the existing model hot H escape predictions. The loss rates are 156% and 83% of the lowest reported seasonal thermal loss rate (Chaffin et al., 2014, 2015; Clarke et al., 2014; Halekas, 2017), indicating that there may be some conditions at Mars in which nonthermal escape dominates thermal escape.

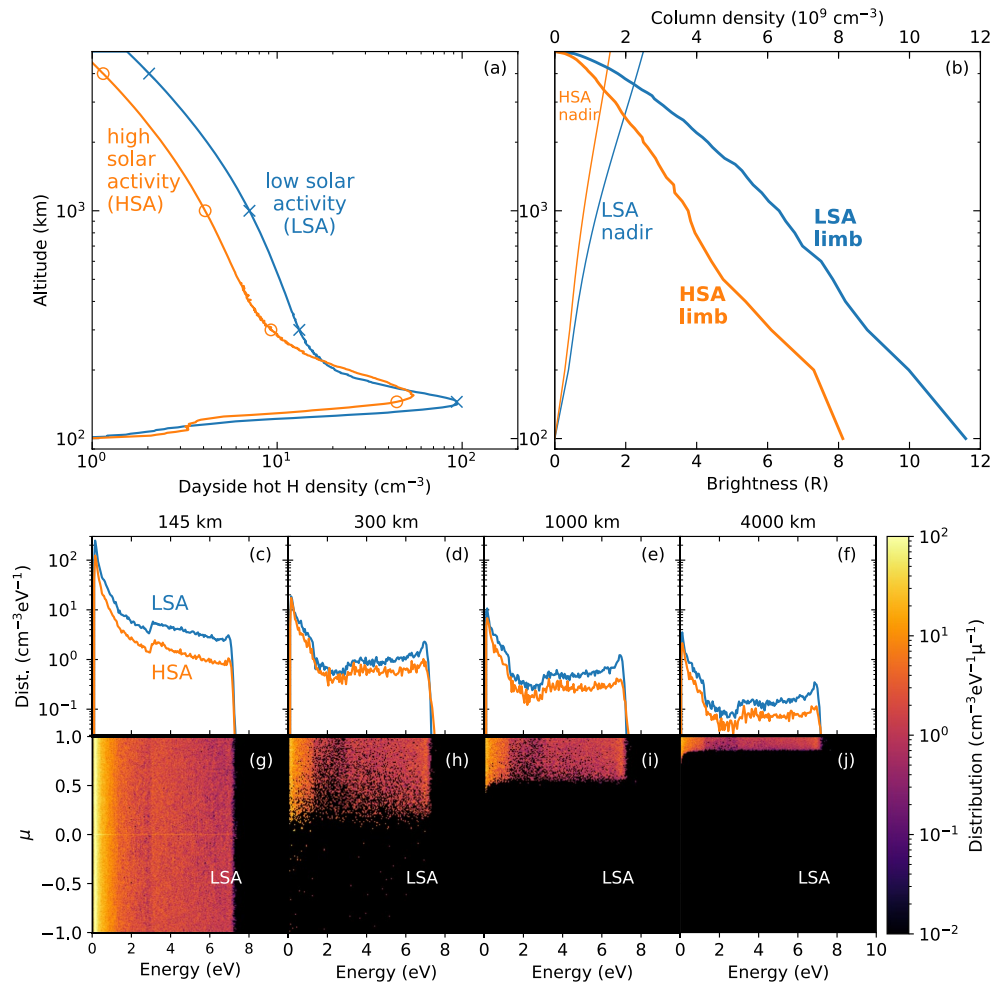
Escape rates are lower under high solar activity conditions, predominantly due to a 35% decrease in escape efficiency (Figure 2). An extended neutral atmosphere under higher solar activity increases the frequency of collisions and rate of thermalization, inhibiting escape. A secondary factor is a 17% decrease in production rate under high solar activity compared to low solar activity, which is due to the lower HCO^+ density around the production rate peak altitudes (100–200 km; Figures 1b and 1c). This anticorrelation of HCO^+ density and solar activity, also seen in other H-bearing ions, including OCOH^+ , which greatly influences HCO^+ production, is due to larger photochemical and escape sinks of H and H_2 under higher solar activity (Fox, 2015). Solar EUV fluxes were higher earlier in solar system history (Ribas et al., 2005; Tu et al., 2015), so our results suggest that escape fluxes from this particular nonthermal mechanism would likely have been smaller in Mars' past than today.

Figure 2a shows output hot H density profiles for a typical model run. Densities peak at altitudes of 143 and 155 km for low and high solar activity conditions, respectively. The increase in the thermosphere scale height under high solar activity suppresses hot atom densities as well as escape. Given our strict definition of hot hydrogen, in which bound hot particles with energies below escape energy are removed from the simulation, despite velocities remaining well above those of thermal particles, observable hot hydrogen densities (of both bound and escaping particles) are likely to be larger than those presented in Figure 2.

An initial estimate of expected brightness profiles resulting from this hot H (Figure 2b) can be obtained assuming that the atmosphere is optically thin with respect to Lyman alpha radiation, which allows us to use the relation:

$$I_i = g \mathcal{N}_i \quad (2)$$

where \mathcal{N}_i is the column density along the line of sight of a spacecraft's remote sensing instrument and g is the photon scattering coefficient ($10^{-3} \text{ photons particle}^{-1} \text{ s}^{-1}$; Anderson & Hord, 1971). For example, assuming



Solar activity	Dayside production rate [s^{-1}]	Loss rate [s^{-1}]	Escape efficiency
Low	6.13×10^{25}	$1.30 \pm 0.01 \times 10^{25}$	0.21
High	5.10×10^{25}	$6.92 \pm 0.04 \times 10^{24}$	0.136

Figure 2. Model predictions of hot hydrogen produced by HCO^+ dissociative recombination. (a) Output average dayside hot H density profiles for a typical simulation, for low (LSA; blue) and high (HSA; orange) solar activity conditions. (b) Predicted brightness profiles for hot H produced by HCO^+ dissociative recombination, for nadir (thin lines) and limb (thick lines) observations, for both low and high solar activity. For limb predictions, the altitude is measured toward the Sun from the subsolar point. The column density, shown on the upper horizontal axis, is multiplied by g (10^{-3} photons particle $^{-1}$ s $^{-1}$) to calculate the brightness (Anderson & Hord, 1971). (c–f) Energy distributions for hot H in one low and one high solar activity simulation, at four different altitudes. (g–j) Energy and direction distributions for hot H in one low solar activity simulation, at the same four altitudes. $\mu = \cos \theta$, where θ is the angle between the particle's path direction and a trajectory pointing directly upwards. Table: Hemispheric hot H production rates via HCO^+ dissociative recombination and calculated global escape rates, for both low and high solar activity conditions. The standard deviation of the mean loss rate is computed from 10 model runs.

a nadir observation at 5,000 km and integrating the low solar activity output densities (Figure 2a) below this altitude, we obtain a brightness of 2.4 Rayleighs (R). Adopting a similar procedure for a limb observation (see Supporting Information S1), we obtain a maximum brightness of 12 R at a spacecraft altitude of 100 km.

Energy distribution functions at a series of altitudes for a typical simulation are shown in Figure 2 (c–j). Panels (g–j) show the distribution of energy and direction of the hot H atoms for one of the low solar activity models, where $\mu = \cos \theta$ and θ is the angle between the atom's direction of motion and a vector pointing radially outward

from the planet. With increasing altitude, the particles transition from moving in all directions to having μ values focused to 1, because most reaching higher altitudes are moving directly upward away from the planet; this is a geometrical effect only. Panels (c–f) show the energy distributions integrated over μ , for both low and high solar activity.

4. Escape Probabilities Close to 100% Above Collisional Atmosphere

We have shown that HCO^+ dissociative recombination is key to a complete understanding of H loss at Mars. This naturally poses the question of the influence of other unstudied nonthermal mechanisms on hot H escape, including the dozens of additional photochemical reactions that produce H above escape energy. For example, the photochemical model of Fox (2015) includes 44 further exothermic reactions with H as a product. Some of these reactions have high excess energies of up to 10.95 eV (H_2^+ dissociative recombination), high column production rates between 80 and 400 km of up to $5.3 \times 10^7 \text{ cm}^{-2} \text{ s}^{-1}$ ($\text{CO}_2^+ + \text{H}_2 \rightarrow \text{OCOH}^+ + \text{H}$), or high peak production rate altitudes of up to 272 km ($\text{H}_2^+ + \text{H}_2 \rightarrow \text{H}_3^+ + \text{H}$), which are all factors that could contribute to considerable escape. The photochemical model of Krasnopolsky (2019) incorporates additional H-producing reactions involving water chemistry, which may become particularly important during some seasonal conditions.

Some photochemical mechanisms have been studied previously. For instance, hot hydrogen produced by the reactions $\text{O}^+ + \text{H}_2 \rightarrow \text{OH}^+ + \text{H}$, $\text{OH}^+ + \text{e}^- \rightarrow \text{O} + \text{H}$, $\text{CO}_2^+ + \text{H}_2 \rightarrow \text{OCOH}^+ + \text{H}$, and $\text{OCOH}^+ + \text{e}^- \rightarrow \text{CO}_2 + \text{H}$ has been simulated for both Mars (Lichtenegger et al., 2006) and Venus (Lammer et al., 2006; McElroy et al., 1982). In addition, the charge exchange reactions of energetic hydrogen ions with oxygen or hydrogen atoms have been modeled to obtain hot H densities at Mars (Lichtenegger et al., 2006; Nagy et al., 1990) and are considered dominant for escape at Venus (Donahue & Hartle, 1992; Hodges, 1999; Hodges & Tinsley, 1981, 1986; Lammer et al., 2006; Rodriguez et al., 1984). Momentum transfer from solar wind penetrating protons to atmospheric H (Halekas et al., 2015) may also produce hot atoms (e.g., Shematovich, 2021). The total escape flux of hydrogen via photochemical and charge exchange sources at Venus is $3.8 \times 10^{25} \text{ s}^{-1}$ (Lammer et al., 2006), which is comparable to our escape fluxes from HCO^+ dissociative recombination (Figure 2). This motivates the investigation of escape at Mars via these and other reactions involving H-bearing ions. In contrast to HCO^+ dissociative recombination, the production rates of some reactions may increase sufficiently with solar activity to overcome the decrease in escape efficiency and therefore may have played a key role in Mars' earlier atmospheric loss.

In order to facilitate future escape estimates of these mechanisms, we produce escape probability profiles for two example particle kinetic energies: 5 and 0.2 eV. The curves, indicating the probability that an H atom born at a certain altitude with a certain kinetic energy will escape, can be used alongside production rate profiles to estimate the production rate of escaping H for different nonthermal mechanisms. We choose an energy of 0.2 eV as a lower limit, as it is just above the escape velocity at 80 km (0.13 eV); 5 eV is a representative value halfway between escape energy and the largest excess energy from an H-producing reaction in Fox's (2015) compilation (10.95 eV), and slightly less than the average kinetic energy imparted to H atoms by HCO^+ dissociative recombination.

To construct the profiles, we use the Monte Carlo model to track the trajectories of 1,000 test particles produced at a single altitude, all with the same initial kinetic energy (5 eV or 0.2 eV). For a series of altitudes between 80 and 400 km, we take the mean escape fraction from four simulations (Figure 3). We calculate the column density of background species above each altitude (N ; Figure 1a), assuming that the column density above 400 km is equal to the sum of the background species' scale heights ($k_b T_n / mg$, where k_b is Boltzmann's constant, m is the molecule's mass, and T_n and g are the neutral temperature and the gravitational acceleration at 400 km) multiplied by their densities at 400 km. The dependence of escape probability on N is independent of the density profiles chosen, so we combine the model results for low and high solar activity for each of the two energies. We then fit the escape probabilities (p) to the form $p = Ae^{(-bN\sigma)}$, where σ is the total O–H cross section at the chosen energy ($3.89 \times 10^{-15} \text{ cm}^2$ for 5 eV and $5.52 \times 10^{-15} \text{ cm}^2$ for 0.2 eV; Zhang et al., 2009). The constant A is equal to the escape probability with no molecules overhead. The constant b is a transparency coefficient, accounting for the fact that a single collision is not necessarily sufficient to thermalize a test particle.

We find that the curves $p = 0.9147e^{(-0.0388 N\sigma)}$ and $p = 0.8133e^{(-0.1225 N\sigma)}$ fit the data for particle populations with initial kinetic energies of 5 and 0.2 eV, respectively. Mapping the column densities to altitudes, the resulting escape probability profiles are shown in Figure 3. Escape probabilities are low below ~ 130 – 150 km and increase

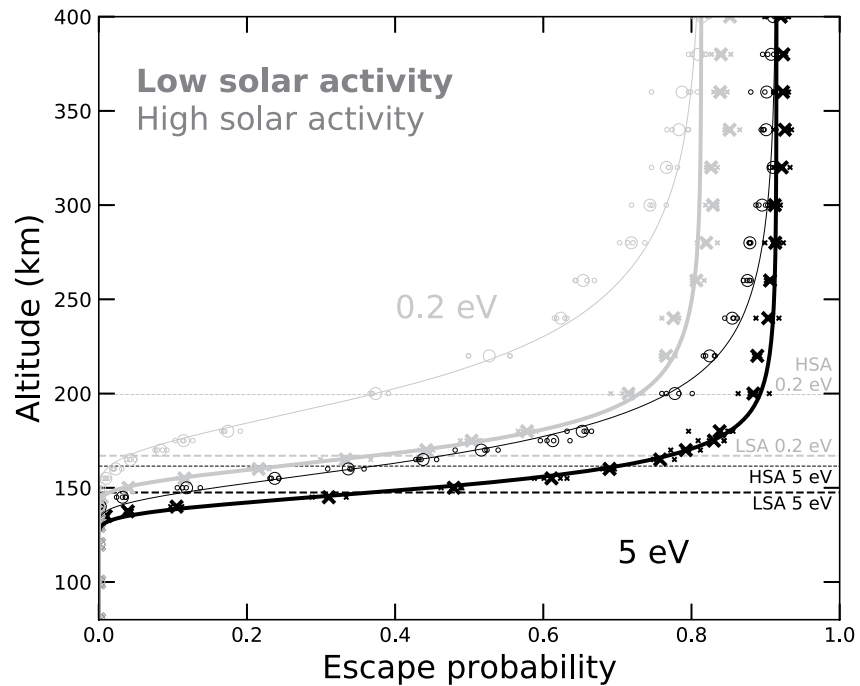


Figure 3. New escape probability profiles for two H population energies and two solar activity conditions. Black lines/symbols and silver lines/symbols are for the 5 and 0.2 eV populations, respectively. Thick lines/crosses and thin lines/circles are for low and high solar activity conditions, respectively. Symbols show the four models run for each altitude (smaller points) and the mean (larger points). Lines are fits of the combined low and high solar activity data for each population energy: $p = 0.9147e^{-0.0388N\sigma}$ for the 5 eV population and $p = 0.8133e^{-0.1225N\sigma}$ for the 0.2 eV population. The curves for each solar activity differ because of the varying overhead column densities (N) with altitude. Horizontal dashed lines indicate the altitude at which the escape probability is equal to $1/e$.

to maximum values of 0.91 and 0.81 for 5 and 0.2 eV populations, respectively, at the uppermost production altitude of 400 km. This is considerably larger than nonthermal oxygen escape probabilities, which are up to 0.4–0.65 (Fox & Hać, 2018; Lillis et al., 2017). Since hydrogen has a much smaller mass compared to oxygen, momentum transfer with CO_2 and O is less effective and more collisions (~ 26 for 5 eV particles and ~ 8 for 0.2 eV particles) are required to reduce a particle's energy to thermalization (Krasnopolsky, 2010). Half of the particles, initially directed upward, all escape, and a large proportion of the half initially directed toward the planet collide frequently enough to be turned around and escape. In other words, A is roughly equivalent to $0.5 + 0.5\alpha$, where α is the planetary albedo with respect to hot hydrogen atoms. We find α values of 0.83 and 0.63 for the 5 and 0.2 eV populations, respectively. While it is known that there is a considerable albedo for $\sim\text{keV}$ -energy H atoms sourced from charge exchange with solar wind protons (e.g., Girazian & Halekas, 2021; Halekas et al., 2015; Kallio & Barabash, 2001), our high albedo results for hot H energies (below ~ 10 eV) indicate the potential for significant net escape of H from photochemical sources operating above ~ 200 km.

5. Applicability to Understanding Hot H Escape at Mars

We have shown that HCO^+ dissociative recombination alone produces a greater proportion of escaping H with respect to thermal hydrogen than some previous modeling estimates of the total nonthermal H loss from photochemical sources ($\leq 5\%$; e.g., Krasnopolsky, 2010; Nagy et al., 1990). Escape through this mechanism has not previously been quantified, and our results suggest it plays a significant (perhaps dominant) role for hot hydrogen escape at Mars.

No direct observations of hot H at Mars have been made to date, but our calculated densities enable predictions of what could be observed in the future (Figure 2b). We predict Lyman alpha brightness from H produced by HCO^+ dissociative recombination of up to 12 R, which is negligible compared to typical H brightness at Mars, on the order of kilo-Rayleighs (e.g., Anderson & Hord, 1971). Therefore, while HCO^+ dissociative recombination

can produce 5% of the nonthermal H escape and around half the total H escape in some seasonal conditions, it is effectively invisible to detection by observational studies, due to the much brighter total H population, most of which is bound to the planet. This highly nonlinear relationship between brightness and escape rate presents a challenge to future missions endeavoring both to detect hot H directly and infer nonthermal escape rates. Further, in previous modeling studies, brightness predictions have matched observations better with the inclusion of hot H alongside a thermal population (e.g., Bhattacharyya et al., 2015), but this requires a much larger brightness contribution from hot H than we predict for the H from HCO⁺ dissociative recombination. Therefore, it is possible that there is another unconsidered hot H-producing mechanism that results in much higher densities and brightnesses, or HCO⁺ dissociative recombination may be even more important than we compute in this study, due to more HCO⁺ in the atmosphere than realized. If this is the case, hot H escape rates would presumably also be much higher.

The individual and cumulative importance of nonthermal processes can be evaluated further in future studies using our new H escape probability profiles, which show that most H produced above the ionospheric peak escapes. An initial escape estimate for a chosen mechanism can be obtained by multiplying the probability by the production rate and integrating over altitude. For example, we can estimate escape for HCO⁺ dissociative recombination and compare to the result described in Figure 2. Due to the energy removed by branching to different electronic states of CO, 77% of the particles initially have a kinetic energy of 7.06 eV and 23% have a kinetic energy of 1.26 eV or less (Rosati et al., 2007). We can approximate escape probabilities for HCO⁺ dissociative recombination as 77% of our new 5 eV profile plus 23% of our 0.2 eV profile, which results in a global loss rate estimate of $1.20 \times 10^{25} \text{ s}^{-1}$ for low solar activity conditions. This is within 8% of our loss rate calculated earlier ($1.30 \times 10^{25} \text{ s}^{-1}$, Figure 2), illustrating the utility of the escape probability profiles for good escape estimates. The marginal underestimation is likely due to a difference in the way that collisions change the velocities of the particles when the initial kinetic energy is slightly different. The Monte Carlo modeling of individual mechanisms that initial estimates highlight as important remains valuable for obtaining escape rates and density and energy distributions.

When considering the loss rates from HCO⁺ dissociative recombination, our model has a few limitations that future versions will address. First, we use one-dimensional input density and temperature profiles, assumed to be uniform across the dayside. This is a simplification, but, assuming an optically thick atmosphere, the total number of HCO⁺ ions in a column should not vary, and the maximum production altitude according to the Chapman function varies across the dayside by no more than one scale height from that with a solar zenith angle of 60°, taken by Fox (2015) to produce the profiles used as inputs in this study. Our model does not capture the effects of seasonal and longer-term density variations: future work will be needed to study important trends. Second, our input profile choices assume an ionopause at 400 km, with no hot H production above this altitude. However, use of our escape probability profiles reveals that, for low solar activity conditions, ~90% of the escaping H produced comes from below 190 km, due to the reaction rate peak around 140 km. Variation of the ionopause above this altitude is therefore unlikely to cause more than a 10% change in values. Third, we do not consider rotational energy, either in the initial HCO⁺ molecule or in the product CO molecule. A similar assumption was made for hot O at Mars in the model of Gröller et al. (2014), given that incorporation of the correct rotational states had a negligible effect on hot O modeling at Venus (Gröller et al., 2010). Including the rotational energy of the CO molecule here would only affect the magnitude of the remaining energy by a factor of 0.1%–1%.

Finally, this model only considers elastic collisions with limited background species. The lack of inelastic collisions may result in some overestimation of particle energies and therefore escape. However, inelastic channels are insignificant for atom–atom collisions at these energies (Lewkow & Kharchenko, 2014), and we follow the assumptions of similar hot H Monte Carlo modeling, which suggests that inelastic atom–molecule collisions are also unimportant at energies below 8 eV (Lammer et al., 2006; Lichtenegger et al., 2006). While estimated H–N₂, H–CO, and H–CO₂ total and differential cross sections, produced using scaling methods from known data, are available (Lewkow & Kharchenko, 2014), we opt instead to use unscaled O–H cross sections for collisions of H with all background species until dedicated cross sections for each collision pair are generated, based on the conclusions of detailed modeling studies performed by Gacesa et al. (2020) for O–CO₂ collisions. This assumption likely affects our results the most, and we will update our model to use the relevant cross sections as they become available.

We simulate collisions with the four most abundant atmospheric neutral species, but not with background H and H₂. The lack of H–H and H–H₂ collisions may have two contrasting effects on our escape results: (a) escape may

be overestimated because of an underestimated collision and thermalization rate, or (b) escape may be underestimated because secondary hot particles are not taken into account. On the one hand, Gu et al. (2020) found that hot helium escape, induced by hot O collisions, decreased by up to 50% when collisions with H and H₂ were incorporated (see their Figure 3 and their Table 2). Part of the observed effect is explained by a reduction in the initial production of hot He atoms by momentum exchange with nonthermal oxygen, presumably because O is more likely to collide with H and H₂ when they are present. This reduction in hot atom production rate is not applicable to the photochemically produced hot hydrogen in our models. The decrease in escape is also attributed in part to a decrease in escape probability as He atoms are thermalized by collisions with H and H₂. The relative importance of these two factors is not shown explicitly by Gu et al. (2020) but in light of this study we might expect the lack of H and H₂ collisions in our model to cause an overestimation of escape by no more than a factor of two and likely less. On the other hand, collisions of hot H with background H could produce secondary hot H particles due to efficient momentum exchange, increasing hot H production and therefore escape (Shematovich, 2004), especially when the primary particles have energies several eV higher than the escape energy, as the majority of those produced by HCO⁺ dissociative recombination do initially. An equivalent process, via collisions with background oxygen, has been included in models of hot O (Gröller et al., 2010; Krestyanikova & Shematovich, 2006; Lichtenegger et al., 2009). We do not expect the overall effect of these two opposing factors to be large because H and H₂ only become dominant ambient species at altitudes above the exobase where collisions are infrequent: they become more important than CO, N₂, and CO₂ only above 240–260 km (360 km) and more important than O only above 340–380 km (and higher) for low (high) solar activity conditions (Fox, 2015), where escape probabilities are already >80%. We conclude that the effect of including H and H₂ as background species would be on the same order of magnitude as the results of some of our other assumptions and does not negate our conclusions, but we intend to incorporate collisions with these species in future model development.

6. Conclusions

Here we have identified HCO⁺ dissociative recombination as a previously overlooked yet important source of escaping hot H at Mars, contributing 3.5%–6.5% of the thermal escape estimate. Modern hydrogen escape rates are insufficient to explain the magnitude of water loss required by D/H ratios, so it is hypothesized that early hydrogen loss was greater (Cangi et al., 2020; Jakosky et al., 2018). However, given that solar EUV fluxes were higher in the past (Ribas et al., 2005; Tu et al., 2015) and our high solar activity simulations result in less escape, we speculate that HCO⁺ dissociative recombination does not explain this effect. Nonetheless, it is possible that other nonthermal mechanisms, such as resonant charge exchange with ionospheric plasma, may have been significant across Mars' lifetime. At Venus, nonthermal loss is dominant due to inhibited thermal escape (Anderson, 1976; Hodges, 1999; Hodges & Tinsley, 1981; Lammer et al., 2006), so we expect that HCO⁺ dissociative recombination, which has also never been explored at that planet, may be very important. This process could also be key at Venus-sized exoplanets with CO₂-rich atmospheres and negligible thermal H loss. Despite the lack of prior work on its effect on escape, HCO⁺ dissociative recombination, along with other nonthermal processes, especially those that produce H above the ionospheric peak, is key to a more comprehensive view of water loss from terrestrial planets.

Data Availability Statement

The model code, output, and plotting scripts used are available in Gregory et al. (2022).

References

- Amerstorfer, U. V., Gröller, H., Lichtenegger, H., Lammer, H., Tian, F., Noack, L., et al. (2017). Escape and evolution of Mars's CO₂ atmosphere: Influence of suprathermal atoms. *Journal of Geophysical Research: Planets*, 122(6), 1321–1337. <https://doi.org/10.1002/2016JE005175>
- Anderson, D. E., Jr. (1976). The Mariner 5 ultraviolet photometer experiment: Analysis of hydrogen Lyman alpha data. *Journal of Geophysical Research*, 81(7), 1213–1216. <https://doi.org/10.1029/JA081i007p01213>
- Anderson, D. E., Jr., & Hord, C. W. (1971). Mariner 6 and 7 ultraviolet spectrometer experiment: Analysis of hydrogen Lyman-alpha data. *Journal of Geophysical Research*, 76(28), 6666–6673. <https://doi.org/10.1029/JA076i028p06666>
- Aoki, S., Vandaele, A. C., Daerden, F., Villanueva, G. L., Liuzzi, G., Thomas, I. R., et al. (2019). Water vapor vertical profiles on Mars in dust storms observed by TGO/NOMAD. *Journal of Geophysical Research: Planets*, 124(12), 3482–3497. <https://doi.org/10.1029/2019JE006109>
- Bhattacharyya, D., Clarke, J. T., Bertaux, J. L., Chaufray, J. Y., & Mayyasi, M. (2015). A strong seasonal dependence in the Martian hydrogen exosphere. *Geophysical Research Letters*, 42(20), 8678–8685. <https://doi.org/10.1002/2015gl065804>

Acknowledgments

This work was supported by NASA Solar System Workings Grant 80NSSC19K0164.

- Bhattacharyya, D., Clarke, J. T., Bertaux, J. L., Chaufray, J. Y., & Mayyasi, M. (2017). Analysis and modeling of remote observations of the Martian hydrogen exosphere. *Icarus*, 281, 264–280. <https://doi.org/10.1016/j.icarus.2016.08.034>
- Bhattacharyya, D., Clarke, J. T., Chaufray, J. Y., Mayyasi, M., Bertaux, J. L., Chaffin, M. S., et al. (2017). Seasonal changes in hydrogen escape from Mars through analysis of HST observations of the Martian exosphere near perihelion. *Journal of Geophysical Research: Space Physics*, 122(11), 756–764. <https://doi.org/10.1002/2017JA024572>
- Bougher, S. W., Blelly, P.-L., Combi, M., Fox, J. L., Mueller-Wodarg, I., Ridley, A., & Roble, R. G. (2008). Neutral upper atmosphere and ionosphere modeling. *Space Science Reviews*, 139(1–4), 107–141. <https://doi.org/10.1007/s11214-008-9401-9>
- Cangi, E. M., Chaffin, M. S., & Deighan, J. (2020). Higher Martian atmospheric temperatures at all altitudes increase the D/H fractionation factor and water loss. *Journal of Geophysical Research: Planets*, 125(12), e2020JE006626. <https://doi.org/10.1029/2020JE006626>
- Chaffin, M. S., Chaufray, J. Y., Deighan, J., Schneider, N. M., Mayyasi, M., Clarke, J. T., et al. (2018). Mars H escape rates derived from MAVEN/IUVS Lyman alpha brightness measurements and their dependence on model assumptions. *Journal of Geophysical Research: Planets*, 123(8), 2192–2210. <https://doi.org/10.1029/2018JE005574>
- Chaffin, M. S., Chaufray, J. Y., Deighan, J., Schneider, N. M., McIlintock, W. E., Stewart, A. I. F., et al. (2015). Three-dimensional structure in the Mars H corona revealed by IUVS on MAVEN. *Geophysical Research Letters*, 42(21), 9001–9008. <https://doi.org/10.1002/2015GL065287>
- Chaffin, M. S., Chaufray, J.-Y., Stewart, I., Montmessin, F., Schneider, N. M., & Bertaux, J.-L. (2014). Unexpected variability of Martian hydrogen escape. *Geophysical Research Letters*, 41(2), 314–320. <https://doi.org/10.1002/2013GL058578>
- Chaffin, M. S., Deighan, J., Schneider, N. M., & Stewart, A. I. F. (2017). Elevated atmospheric escape of atomic hydrogen from Mars induced by high-altitude water. *Nature Geoscience*, 10(3), 174–178. <https://doi.org/10.1038/NGEO2887>
- Chaffin, M. S., Kass, D. M., Aoki, S., Fedorova, A. A., Deighan, J., Connour, K., et al. (2021). Martian water loss to space enhanced by regional dust storms. *Nature Astronomy*, 5(10), 1036–1042. <https://doi.org/10.1038/s41550-021-01425-w>
- Chaufray, J. Y., Bertaux, J. L., Leblanc, F., & Quémerais, E. (2008). Observation of the hydrogen corona with SPICAM on Mars Express. *Icarus*, 195(2), 598–613. <https://doi.org/10.1016/j.icarus.2008.01.009>
- Chaufray, J. Y., Gonzalez-Galindo, F., Lopez-Valverde, M. A., Forget, F., Quémerais, E., Bertaux, J., et al. (2021). Study of the hydrogen escape rate at Mars during Martian years 28 and 29 from comparisons between SPICAM/Mars express observations and GCM-LMD simulations. *Icarus*, 353, 113498. <https://doi.org/10.1016/j.icarus.2019.113498>
- Chaufray, J. Y., Modolo, R., Leblanc, F., Chanteur, G., Johnson, R. E., & Luhmann, J. G. (2007). Mars solar wind interaction: Formation of the Martian corona and atmospheric loss to space. *Journal of Geophysical Research*, 112(E9), E09009. <https://doi.org/10.1029/2007JE002915>
- Clarke, J. T., Bertaux, J. L., Chaufray, J. Y., Gladstone, G. R., Quemerais, E., Wilson, J. K., & Bhattacharyya, D. (2014). A rapid decrease of the hydrogen corona of Mars. *Geophysical Research Letters*, 41(22), 8013–8020. <https://doi.org/10.1002/2014GL061803>
- Donahue, T. M., & Hartle, R. E. (1992). Solar cycle variations in H⁺ and D⁺ densities in the Venus ionosphere: Implications for escape. *Geophysical Research Letters*, 19(24), 2449–2452. <https://doi.org/10.1029/92GL02927>
- Fedorova, A., Bertaux, J., Betsis, D., Montmessin, F., Korablev, O., Maltagliati, L., & Clarke, J. (2018). Water vapor in the middle atmosphere of Mars during the 2007 global dust storm. *Icarus*, 300, 440–457. <https://doi.org/10.1016/j.icarus.2017.09.025>
- Fedorova, A., Montmessin, F., Korablev, O., Luginin, M., Trokhimovskiy, A., Belyaev, D. A., et al. (2020). Stormy water on Mars: The distribution and saturation of atmospheric water during the dusty season. *Science*, 367(6475), 297–300. <https://doi.org/10.1126/science.aay9522>
- Fox, J. L. (2015). The chemistry of protonated species in the Martian ionosphere. *Icarus*, 252, 366–392. <https://doi.org/10.1016/j.icarus.2015.01.010>
- Fox, J. L., & Hač, A. B. (2018). Escape of O(³P), O(¹D), and O(¹S) from the Martian atmosphere. *Icarus*, 300(2), 411–439. <https://doi.org/10.1016/j.icarus.2017.08.041>
- Gacesa, M., Lillis, R. J., & Zahnle, K. J. (2020). O(³P) + CO₂ scattering cross-sections at superthermal collision energies for planetary aeronomy. *Monthly Notices of the Royal Astronomical Society*, 491(4), 5650–5659. <https://doi.org/10.1093/mnras/stz3366>
- Galli, A., Wurz, P., Lammer, H., Lichtenegger, H. I. M., Lundin, R., Barabash, S., et al. (2006). The hydrogen exospheric density profile measured with ASPERA-3/NPD. *Space Science Reviews*, 126(1–4), 447–467. <https://doi.org/10.1007/s11214-006-9089-7>
- Girazian, Z., & Halekas, J. (2021). Precipitating solar wind hydrogen at Mars: Improved calculations of the backscatter and albedo with MAVEN observations. *Journal of Geophysical Research: Planets*, 126(2), e2020JE006666. <https://doi.org/10.1029/2020JE006666>
- Gregory, B. S., Elliott, R. D., Deighan, J., Gröller, H., Chaffin, M. S., & Chirakkil, K. (2022). bethangregory/corona3d2020: corona3d2020v1.0.5 (v1.0.5). <https://doi.org/10.5281/zenodo.7464345>
- Gröller, H., Lammer, H., Lichtenegger, H. I. M., Pflieger, M., Dutuit, O., Sematovich, V. I., et al. (2012). Hot oxygen atoms in the Venus nightside exosphere. *Geophysical Research Letters*, 39(3), L03202. <https://doi.org/10.1029/2011GL050421>
- Gröller, H., Lichtenegger, H., Lammer, H., & Sematovich, V. I. (2014). Hot oxygen and carbon escape from the Martian atmosphere. *Planetary and Space Science*, 98, 93–105. <https://doi.org/10.1016/j.pss.2014.01.007>
- Gröller, H., Sematovich, V. I., Lichtenegger, H. I. M., Lammer, H., Pflieger, M., Kulikov, Y. N., et al. (2010). Venus' atomic hot oxygen environment. *Journal of Geophysical Research*, 115(E12), E12017. <https://doi.org/10.1029/2010JE003697>
- Gu, H., Cui, J., Niu, D., He, Z., & Li, K. (2020). Monte Carlo calculations of helium escape on Mars via energy transfer from hot oxygen atoms. *The Astrophysical Journal*, 902(2), 121. <https://doi.org/10.3847/1538-4357/abb6e9>
- Halekas, J. S. (2017). Seasonal variability of the hydrogen exosphere of Mars. *Journal of Geophysical Research: Planets*, 122(5), 901–911. <https://doi.org/10.1002/2017JE005306>
- Halekas, J. S., Lillis, R. J., Mitchell, D. L., Cravens, T. E., Mazelle, C., Connerney, J. E. P., et al. (2015). MAVEN observations of solar wind hydrogen deposition in the atmosphere of Mars. *Geophysical Research Letters*, 42(21), 8901–8909. <https://doi.org/10.1002/2015GL064693>
- Heavens, N. G., Kleinböhl, A., Chaffin, M. S., Halekas, J. S., Kass, D. M., Hayne, P. O., et al. (2018). Hydrogen escape from Mars enhanced by deep convection in dust storms. *Nature Astronomy*, 2, 126–132. <https://doi.org/10.1038/s41550-017-0353-4>
- Hodges, R. R., Jr. (1994). Monte Carlo simulation of the terrestrial hydrogen exosphere. *Journal of Geophysical Research*, 99(A12), 23229–23247. <https://doi.org/10.1029/94JA02183>
- Hodges, R. R., Jr. (1999). An exospheric perspective of isotopic fractionation of hydrogen on Venus. *Journal of Geophysical Research*, 104(E4), 8463–8471. <https://doi.org/10.1029/1999JE900006>
- Hodges, R. R., Jr., & Tinsley, B. A. (1981). Charge exchange in the Venus ionosphere as the source of the hot exospheric hydrogen. *Journal of Geophysical Research*, 86(A9), 7649–7656. <https://doi.org/10.1029/JA086iA09p07649>
- Hodges, R. R., Jr., & Tinsley, B. A. (1986). The influence of charge exchange on the velocity distribution of hydrogen in the Venus exosphere. *Journal of Geophysical Research*, 91(A12), 13649–13658. <https://doi.org/10.1029/JA091iA12p13649>
- Jakosky, B. M., Brain, D., Chaffin, M., Curry, S., Deighan, J., Grebowsky, J., et al. (2018). Loss of the Martian atmosphere to space: Present-day loss rates determined from MAVEN observations and integrated loss through time. *Icarus*, 315, 146–157. <https://doi.org/10.1016/j.icarus.2018.05.030>

- Johnson, R. E., Combi, M. R., Fox, J. L., Ip, W. H., Leblanc, F., McGrath, M. A., et al. (2008). Exospheres and atmospheric escape. *Space Science Reviews*, 139(1–4), 355–397. <https://doi.org/10.1007/s11214-008-9415-3>
- Kallio, E., & Barabash, S. (2001). Atmospheric effects of precipitating energetic hydrogen atoms on the Martian atmosphere. *Journal of Geophysical Research*, 106(A1), 165–177. <https://doi.org/10.1029/2000JA002003>
- Krasnopolsky, V. A. (2002). Mars' upper atmosphere and ionosphere at low, medium, and high solar activities: Implications for evolution of water. *Journal of Geophysical Research*, 107(E12), 11–11–11. <https://doi.org/10.1029/2001je001809>
- Krasnopolsky, V. A. (2010). Solar activity variations of thermospheric temperatures on Mars and a problem of CO in the lower atmosphere. *Icarus*, 207(2), 638–647. <https://doi.org/10.1016/j.icarus.2009.12.036>
- Krasnopolsky, V. A. (2019). Photochemistry of water in the Martian thermosphere and its effect on hydrogen escape. *Icarus*, 321, 62–70. <https://doi.org/10.1016/j.icarus.2018.10.033>
- Krestyanikova, M., & Shematovich, V. (2006). Stochastic models of hot planetary and satellite coronas: A hot oxygen corona of Mars. *Solar System Research*, 40(5), 384–392. <https://doi.org/10.1134/S0038094606050030>
- Lammer, H., Lichtenegger, H. I. M., Biernat, H. K., Erkaev, N. V., Arshukova, I. L., Kolb, C., et al. (2006). Loss of hydrogen and oxygen from the upper atmosphere of Venus. *Planetary and Space Science*, 54(13–14), 1445–1456. <https://doi.org/10.1016/j.pss.2006.04.022>
- Lammer, H., Lichtenegger, H. I. M., Kolb, C., Ribas, I., Guinan, E. F., Abart, R., & Bauer, S. J. (2003). Loss of water from Mars: Implications for the oxidation of the soil. *Icarus*, 165(1), 9–25. [https://doi.org/10.1016/S0019-1035\(03\)00170-2](https://doi.org/10.1016/S0019-1035(03)00170-2)
- Lewkow, N. R., & Kharchenko, V. (2014). Precipitation of energetic neutral atoms and induced non-thermal escape fluxes from the Martian atmosphere. *The Astrophysical Journal*, 790(2), 98. <https://doi.org/10.1088/0004-637X/790/2/98>
- Lichtenegger, H., Gröller, H., Lammer, H., Kulikov, Y. N., & Shematovich, V. I. (2009). On the elusive hot oxygen corona of Venus. *Geophysical Research Letters*, 36(10), L10204. <https://doi.org/10.1029/2009GL037575>
- Lichtenegger, H., Lammer, H., Kulikov, Y. N., Kazeminejad, S., Molina-Cuberos, G. H., Rodrigo, R., et al. (2006). Effects of low energetic neutral atoms on Martian and Venusian dayside exospheric temperature estimations. *Space Science Reviews*, 126(1–4), 469–501. <https://doi.org/10.1007/s11214-006-9082-1>
- Lillis, R. J., Deighan, J., Fox, J. L., Bougher, S. W., Lee, Y., Combi, M. R., et al. (2017). Photochemical escape of oxygen from Mars: First results from MAVEN in situ data. *Journal of Geophysical Research: Space Physics*, 122(3), 3815–3836. <https://doi.org/10.1002/2016JA023525>
- Matta, M., Withers, P., & Mendillo, M. (2013). The composition of Mars' topside ionosphere: Effects of hydrogen. *Journal of Geophysical Research: Space Physics*, 118(5), 2681–2693. <https://doi.org/10.1002/jgra.50104>
- McElroy, M. B., Prather, M. J., & Rodriguez, J. M. (1982). Escape of hydrogen from Venus. *Science*, 215(4540), 1614–1615. <https://doi.org/10.1126/science.215.4540.1614>
- Nagy, A., Kim, J., & Cravens, T. (1990). Hot hydrogen and oxygen atoms in the upper atmospheres of Venus and Mars: Distribution of hot hydrogen and oxygen calculated by a theoretical model. *Annales Geophysicae*, 8(4), 251–256.
- Nair, H., Allen, M., Anbar, A. D., Yung, Y. L., & Clancy, R. T. (1994). A photochemical model of the Martian atmosphere. *Icarus*, 111(1), 124–150. <https://doi.org/10.1006/icar.1994.1137>
- Nearly, L., Daerden, F., Aoki, S., Whiteway, J., Clancy, R. T., Smith, M., et al. (2020). Explanation for the increase in high-altitude water on Mars observed by NOMAD during the 2018 global dust storm. *Geophysical Research Letters*, 47(7), e2019GL084354. <https://doi.org/10.1029/2019GL084354>
- Owen, T., Maillard, J. P., de Bergh, C., & Lutz, B. L. (1988). Deuterium on Mars: The abundance of HDO and the value of D/H. *Science*, 240(4860), 1767–1770. <https://doi.org/10.1126/science.240.4860.1767>
- Ribas, I., Guinan, E. F., Güdel, M., & Audard, M. (2005). Evolution of the solar activity over time and effects on planetary atmospheres. I. High-energy irradiances (1–1700 Å). *The Astrophysical Journal*, 622(1), 680–694. <https://doi.org/10.1086/427977>
- Rodriguez, J. M., Prather, M. J., & McElroy, M. B. (1984). Hydrogen on Venus: Exospheric distribution and escape. *Planetary and Space Science*, 32(10), 1235–1255. [https://doi.org/10.1016/0032-0633\(84\)90067-9](https://doi.org/10.1016/0032-0633(84)90067-9)
- Rosati, R. E., Skrzypkowski, M. P., Johnsen, R., & Golde, M. F. (2007). Yield of excited CO molecules from dissociative recombination of HCO⁺ and HOC⁺ ions with electrons. *The Journal of Chemical Physics*, 126(15), 154302. <https://doi.org/10.1063/1.2715943>
- Shaposhnikov, D. S., Medvedev, A. S., Rodin, A. V., & Hartogh, P. (2019). Seasonal water “pump” in the atmosphere of Mars: Vertical transport to the thermosphere. *Geophysical Research Letters*, 46(8), 4161–4169. <https://doi.org/10.1029/2019GL082839>
- Shematovich, V. I. (2004). Stochastic models of hot planetary and satellite coronas. *Solar System Research*, 38(1), 28–38. <https://doi.org/10.1023/B:SOLS.0000015153.66874.25>
- Shematovich, V. I. (2013). Suprathermal oxygen and hydrogen atoms in the upper Martian atmosphere. *Solar System Research*, 47(6), 437–445. <https://doi.org/10.1134/S0038094613060087>
- Shematovich, V. I. (2021). Atmospheric loss of atomic oxygen during proton aurorae on Mars. *Solar System Research*, 55(4), 324–334. <https://doi.org/10.1134/S0038094621040079>
- Stone, S. W., Yelle, R. V., Benna, M., Lo, D. Y., Elrod, M. K., & Mahaffy, P. R. (2020). Hydrogen escape from Mars is driven by seasonal and dust storm transport of water. *Science*, 370(6518), 824–831. <https://doi.org/10.1126/science.aba5229>
- Tu, L., Johnstone, C. P., Güdel, M., & Lammer, H. (2015). The extreme ultraviolet and X-ray Sun in Time: High-energy evolutionary tracks of a solar-like star. *Astronomy & Astrophysics*, 577, L3. <https://doi.org/10.1051/0004-6361/201526146>
- Villanueva, G. L., Mumma, M. J., Novak, R. E., Käufel, H. U., Hartogh, E. T. P., Tokunaga, A., et al. (2015). Strong water isotopic anomalies in the Martian atmosphere: Probing current and ancient reservoirs. *Science*, 348(6231), 218–221. <https://doi.org/10.1126/science.aaa3630>
- X-5 Monte Carlo Team. (2003). MCNP—A general Monte Carlo n-particle transport code, version 5. Volume I: Overview and theory, LA-UR-03-1987 [Computer software manual]. MCNP. Retrieved from https://mcnp.lanl.gov/pdf_files/la-ur-03-1987.pdf
- Zhang, P., Kharchenko, V., Jamieson, M. J., & Dalgarno, A. (2009). Energy relaxation in collisions of hydrogen and deuterium with oxygen atoms. *Journal of Geophysical Research*, 114(A7), A07101. <https://doi.org/10.1029/2009JA014055>